MOLTEN SALT-DRIVEN MXENE $Ti_3C_2T_X$ NANOSHEETS BASED PVDF-HFP COMPOSITES FOR ELECTROMAGNETIC INTERFERENCE SHIELDING WITH ENHANCED MECHANICAL PROPERTIES AND FLAME RETARDANCY

TỔNG HỢP VẬT LIỆU PVDF-HFP COMPOSITE CHE CHẮN NHIỄU ĐIỆN TỪ SỬ DỤNG TẤM NANO MXENE $Ti_3C_2T_X$ ĐƯỢC ĐIỀU CHẾ BẰNG MUỐI NÓNG CHẢY ĐỂ TĂNG CƯỜNG TÍNH CHẤT CƠ HỌC VÀ KHẢ NĂNG CHỐNG CHÁY

Ha Thi Nguyen[1], Tuong Vi Thi Tran[2], Van Thanh Vu[3], Van Vinh Nguyen[3], Van Tho Nguyen[4], Minh Canh Vu[3]*, Thi Kieu Lien Mai[5]*

[1]Industrial University of Ho Chi Minh City, Vietnam
[2]Nguyen Tat Thanh University, Vietnam
[3]The University of Danang - Advanced Institute of Science and Technology, Vietnam
[4]The University of Danang - VN-UK Institute for Research and Executive Education, Vietnam
[5]The University of Danang - University of Science and Education, Vietnam

*Corresponding author: mtklien@ued.udn.vn; vmcanh@aist.udn.vn

(Received: September 19, 2025; Revised: October 26, 2025; Accepted: September 15, 2025)

DOI: 10.31130/ud-jst.2025.23(11).470E

Abstract - The surge of portable and wearable electronics demands lightweight, flexible, multifunctional electromagnetic interference (EMI) shielding materials with mechanical strength and fire resistance. We fabricated composite films reinforced with nanosheets via chloride-based molten salt etching. These MXene/PVDF-HFP (MX/P) films showed a tunable balance between stiffness and flexibility. Although toughness declined with higher MXene content, they retained foldability and integrity under severe deformation. Electrical conductivity rose sharply from 1.7 S m^{-1} at 10 wt% to >2.1×10^3 S m^{-1} at 50 wt%, while EMI shielding effectiveness reached \~36 dB across 8.2–12.4 GHz (>99.97% attenuation). Tests with smartwatches and EMF meters confirmed strong shielding of wireless signals. MXene also improved flame retardancy, enabling self-extinguishing behavior. These results identify MX/P composites as flexible, robust, and multifunctional materials for next-generation EMI shielding in wearable and aerospace technologies.

Key words - Electromagnetic Interference Shielding; MXene Nanosheets; PVDF-HFP Polymer Composites; Mechanical Flexibility; Flame retardancy

Tóm tắt - Sự bùng nổ thiết bị di động và đeo được đòi hỏi vật liệu che chắn nhiễu điện từ (EMI) nhẹ, linh hoạt, đa chức năng nhưng vẫn bền và chống cháy. Chúng tôi chế tạo màng composite MXene/PVDF-HFP (MX/P) gia cường bởi nanosheet bằng quy trình khắc muối nóng chảy gốc clorua. Màng cho phép điều chỉnh cân bằng giữa độ cứng và độ linh hoạt; dù độ dai giảm khi tăng hàm lượng MXene, chúng vẫn gập được và giữ nguyên tính toàn vẹn dưới biến dạng lớn. Độ dẫn điện tăng mạnh từ 1,7 S·m^{-1} (10 wt%) lên >2,1×10^3 S·m^{-1} (50 wt%). Hiệu quả che chắn đạt ~36 dB trong dải 8,2–12,4 GHz, tương ứng suy giảm >99,97% năng lượng nhiễu. Thử nghiệm với đồng hồ thông minh và máy đo EMF xác nhận khả năng chặn mạnh tín hiệu không dây. MXene đồng thời nâng cao tính chống cháy, tạo hành vi tự tắt. Các kết quả chứng minh MX/P là vật liệu linh hoạt, bền chắc và đa dụng, phù hợp cho che chắn EMI thế hệ mới trong thiết bị đeo và ứng dụng hàng không vũ trụ.

Từ khóa - Che chắn nhiễu điện từ; Tấm nano MXene; polymer composite; Tính linh hoạt cơ học; Tính chống cháy

1. Introduction

The rapid expansion of wireless communication systems, Internet-of-Things (IoT) devices, and wearable electronics has brought unprecedented convenience but also heightened concerns regarding electromagnetic interference (EMI) [1]. Uncontrolled electromagnetic radiation not only degrades device performance and data security but also poses health risks to users, highlighting the urgent need for reliable EMI shielding materials. Conventional metal foils and conductive polymers have served this purpose. However, their high density, poor flexibility, corrosion susceptibility, and limited multifunctionality constrain their integration into portable and wearable systems [2]. Thus, lightweight, flexible, and multifunctional EMI shielding materials are urgently required [3].

Two-dimensional (2D) transition metal carbides and nitrides, known as MXenes, have emerged as promising candidates owing to their metallic conductivity, tunable surface terminations, and layered morphology that enhances both reflection and absorption mechanisms [4, 5]. Among them, $Ti_3C_2T_x$ has attracted particular attention due to its high electrical conductivity and ease of chemical modification. Nevertheless, conventional HF-based etching routes for MXene synthesis pose safety hazards, environmental concerns, and limitations in scalability [6]. To address these issues, chloride-based molten salt etching has been recently proposed as a fluoride-free strategy, enabling large-scale synthesis of $Ti_3C_2T_x$ with expanded interlayer spacing and chloride terminations that facilitate subsequent functionalization [7].

Incorporating MXenes into polymer matrices offers an effective route to combine electrical performance with mechanical compliance. Poly(vinylidene fluoride-co-

hexafluoropropylene) (PVDF-HFP), in particular, is an attractive host polymer owing to its low density, high flexibility, chemical stability, and processability [8]. Embedding MXenes within PVDF-HFP can yield hybrid films that not only exhibit excellent EMI shielding but also maintain foldability, toughness, and additional properties such as flame retardancy. Despite this potential, systematic studies on chloride-etched MXene/polymer composites remain scarce, especially concerning the interplay among electrical conductivity, EMI shielding performance, mechanical properties, and thermal stability against combustion.

Here, we present the fabrication and characterization of MXene/PVDF-HFP (MXn/P) composite films prepared by molten-salt-etched $Ti_3C_2T_x$ nanosheets. By varying MXene loadings (10–50 wt%), we reveal a percolation-driven transition in electrical conductivity, a corresponding boost in EMI SE, and tunable mechanical performance. Real-world EMI shielding demonstrations and flame-retardant tests further underscore the multifunctionality of these films, highlighting their potential for next-generation flexible and wearable shielding applications.

2. Experimental Section

2.1. Materials

Titanium aluminium carbide 312 powder (MAX, ≤100 µm), ammonium persulfate ($(NH_4)_2S_2O_8$, CAS No. 7727-54-0), copper chloride ($CuCl_2$, CAS # 7447-39-4), sodium chloride (NaCl, CAS # 7647-14-5), and potassium chloride (KCl, CAS # 7447-40-7) were purchased from Sigma-Aldrich. Hydrochloric acid (HCl, 37-38 wt%) was purchased from Xilong, China. Poly(Vinylidene Fluoride-Co-Hexafluoropropylene) (PVDF-HFP) with M_w 400,000 and M_n 130,000 pellets was purchased from Sigma-Aldrich (USA). N, N-Dimethylformamide (DMF) was purchased from Sigma-Aldrich (USA).

2.2. Synthesis of $Ti_3C_2T_x$ Mxene powder

To synthesize MXene $Ti_3C_2T_x$, Ti_3AlC_2 powder was employed as the precursor, and a chloride-based molten salt mixture ($CuCl_2$/NaCl/KCl) was selected as the etching medium. The precursor and salts were weighed in a molar ratio of 1:3:2:2, respectively, and blended thoroughly for about 10 min to obtain a uniform mixture [9]. The homogenized powder was then transferred into an alumina crucible and placed in a tubular furnace under continuous N_2 flow. The sample was heated from room temperature to 680 °C at a heating rate of 4 °C/min and kept at this temperature for 24 h.

After cooling, the obtained reddish-brown solid was rinsed several times with deionized water to remove residual salts and subsequently collected by vacuum filtration using an anodic aluminum oxide (AAO) membrane. To eliminate possible copper residues, the filtered product was further treated with an aqueous solution of $(NH_4)_2S_2O_8$. Finally, the powders were repeatedly washed with deionized water, filtered, and dried in a vacuum oven at 80°C overnight, resulting in $Ti_3C_2T_x$ MXene.

2.3. Fabrication of MX_n/P composites

The fabrication route of MXene/PVDF-HFP (MX_n/P) composite films is schematically presented in Figure 1.

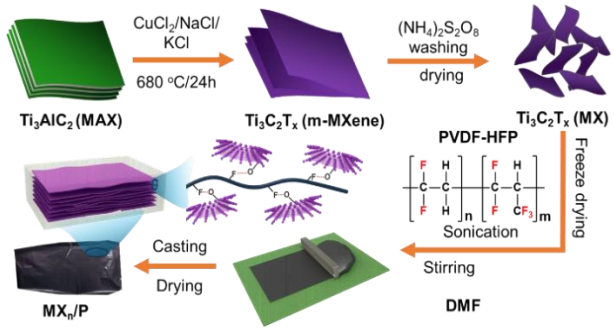

Figure 1. *Schematic diagram of the preparation process of MXene by molten salting etching and fabrication of MX_n/P composite films*

In a typical procedure, a predetermined amount of MXene (Table 1) was introduced into DMF. Following the dispersion step, poly(vinylidene fluoride-co-hexafluoropropylene) (PVDF-HFP) granules were added into the MXene suspension in an amount corresponding to 10 wt% relative to the DMF solvent. The mixture was then sealed to avoid solvent evaporation and stirred magnetically at 70 °C for 4 h, allowing complete polymer dissolution and intimate mixing with the dispersed MXene nanosheets.

The homogeneous viscous solution obtained after mixing was subsequently cast onto a pre-cleaned glass substrate with a pre-adjusted wet thickness. A stainless-steel blade was employed to spread the solution manually, ensuring an even coating layer across the substrate surface. The cast films were then dried at 80°C for 2 h under ambient pressure to remove residual DMF and to induce polymer solidification. This process yielded free-standing MX_n/P composite films with a final thickness 8-10µm. To explore the influence of filler loading on the structural and functional properties of the composites, films were prepared with different MXene contents of 10, 20, 30, and 50 wt% relative to PVDF-HFP.

Table 1. *Compositions and controlled thickness of solutions.*

Sample name	MX (g)	MX (wt%)	PVDF-HFP (g)	DMF (g)	Thickness of solution (µm)	Thickness of film (µm)
MX_{10}/P	0.06	10	0.54	4.86	0.21	8
MX_{20}/P	0.12	20	0.48	4.32	0.185	8
MX_{30}/P	0.18	30	0.42	3.78	0.135	8
MX_{50}/P	0.3	50	0.3	2.7	0.135	10

2.4. Characterizations

The crystal structure of the prepared samples was examined by X-ray diffraction (XRD, Rigaku D8), while their surface morphology was analyzed by scanning electron microscopy (SEM, Helios 5 PFIB CXe DualBeam, Fisher Thermal Scientific) and transmission electron microscopy (TEM, JEOL JEM-F200 Multi-purpose Electron Microscope). Mechanical properties of the composites were conducted on films with dimensions of 8 × 30 mm^2 using a Mecmesin ILC-S 2500N mechanical strength analyzer. The tests were performed at a strain rate

of 10 mm/min at room temperature (30-35 °C). The electrical conductivity (σ) of the films was calculated using the relation:

$$\sigma = \frac{1}{dR_s} \quad (1)$$

where d represents the film thickness and R_s is the sheet resistance. Measurements were conducted with a Four-Point Probe Plus system (OSSILA BV, UK). For the demonstration of electrical conductivity, a film strip with dimensions of 3 × 1.5 cm as the electrode was connected to a 3 V battery to illuminate a light bulb, and photographs were taken to visualize the effect of varying MXene loading.

The EMI shielding effectiveness of PMA composites was evaluated across the X-band frequency range (8.20-12.4 GHz) with a vector network analyzer (N5224A). For EMI shielding assessment, square films (3×3 cm) were positioned between a high-frequency radiometer (EMF Meter, Shenzhen Mystech Electronics Co., China) and a laptop computer, and the shielding effect was recorded photographically.

3. Results and discussion

3.1. Morphology and crystallinity

As illustrated in Figure 1, the reaction pathway occurs when Ti_3AlC_2 is treated with $CuCl_2$ at 680 °C to produce $Ti_3C_2T_x$ MXene. At this temperature, $CuCl_2$ in combination with NaCl/KCl forms a molten salt medium. Within this environment, the Al layers in Ti_3AlC_2 are oxidized to Al^{3+} ions, while Cu^{2+} ions are reduced to metallic Cu that nucleates on the MXene surface. Simultaneously, volatile $AlCl_3$ is generated, which promotes the expansion and delamination of the MXene sheets (eq. 2). In addition, an excess of Cu^{2+} interacts with exposed Ti atoms, leading to the deposition of Cu metal and the incorporation of chloride anions that stabilize the structure by forming $Ti_3C_2Cl_2$ (eq. 3). The resulting $Ti_3C_2Cl_2$ powders were subsequently immersed in ammonium persulfate (APS) solution, which oxidatively removed residual Cu particles while simultaneously introducing oxygen-containing functional groups onto the MXene surface.

$$Ti_3AlC_2 + 3/2CuCl_2 \xrightarrow{NaCl/KCl} Ti_3C_2 + AlCl_3 + 3/2Cu \quad (2)$$

$$Ti_3C_2 + CuCl_2 \xrightarrow{NaCl/KCl} Ti_3C_2Cl_2 + Cu \quad (3)$$

Morphological analysis further indicates the differences between pristine and treated samples. SEM revealed the characteristic accordion-like morphology of layered MAX (Figure 2a). TEM provided additional insights: thin, transparent $Ti_3C_2T_x$ nanosheet with lateral dimensions of ~1 µm and well-defined edges were observed (Figure 2b). Selected area electron diffraction (SAED) showed sharp hexagonal reflections, indicating that the MXene preserved crystallinity (inset in Figure 3b). The structural evolution of the materials was further examined by XRD, as shown in Figure 2c. For the pristine Ti_3AlC_2 MAX phase, a series of sharp diffraction peaks corresponding to its well-defined crystalline structure are observed. After molten-salt etching with $CuCl_2$/NaCl/KCl, most of the non-(00l) reflections of Ti_3AlC_2 vanish, and only low-intensity broad peaks remain, with the (002) reflection of $Ti_3C_2T_x$ at 2θ of 6.76° becoming dominant [10, 11]. This transformation confirms the selective removal of Al layers from Ti_3AlC_2 and the successful formation of layered Ti_3C_2 MXene nanosheets [11]. The shift of the (002) peak to a lower angle compared to the parent MAX phase also indicates an increase in interlayer spacing, consistent with the expansion caused by chloride terminations and the escape of $AlCl_3$ during etching. Figure 2d presents the XRD patterns of $Ti_3C_2T_x$ incorporated into poly(vinylidene fluoride-co-hexafluoropropylene) (PVDF-HFP) matrices at different filler loadings (10, 30, and 50 wt%). In all cases, the characteristic (002) reflection of MXene is retained, demonstrating that the layered structure remains intact after mixing with the polymer. However, the peak gradually broadens and shifts slightly with increasing MXene content. Such broadening suggests a reduction in the average coherent domain size, which can be attributed to improved exfoliation and partial disordering of MXene layers within the polymer host. Meanwhile, the shift of the (002) reflection reflects subtle variations in interlayer spacing, which likely arise from polymer chain intercalation between MXene sheets or from steric constraints imposed by the surrounding PVDF-HFP matrix [12]. At higher loadings (30–50 wt%), the peak sharpening becomes more pronounced, indicating that strong interfacial interactions between MXene and PVDF-HFP lead to constrained stacking and possible turbostratic disorder.

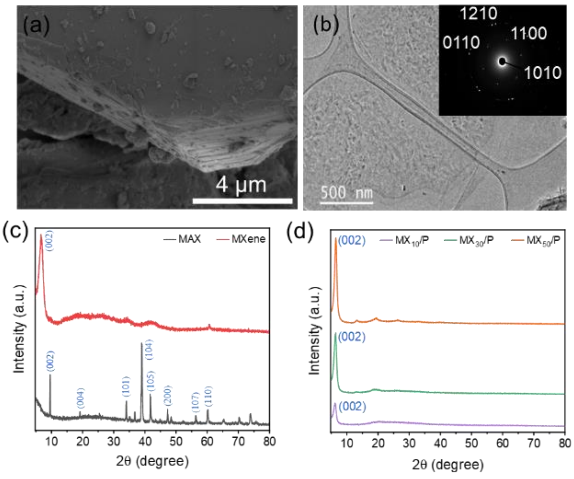

Figure 2. *(a) SEM image of Max, (b) TEM image of Mxene, (c) XRD of MAX and MXene, (d) XRD of MX_n/P films*

3.2. Mechanical properties

The tensile responses of neat PVDF-HFP and MXene/PVDF-HFP composites with varying MXene loadings are shown in Figure 3. Neat PVDF-HFP exhibited the highest tensile strength (49.2 MPa) and elongation at break (≈16.8%), resulting in a toughness of 6.47 $MJ \cdot m^{-3}$. This balance of strength and ductility highlights the intrinsic flexibility of the polymer matrix. With the incorporation of 10 wt% MXene, tensile strength decreased to 32.8 MPa, and strain at break dropped sharply to ≈6.4%. The overall toughness declined to 1.38 $MJ \cdot m^{-3}$, suggesting that although MXene stiffens the composite, it introduces stress concentration sites that promote early fracture. Further increases in MXene content led to a pronounced stiffening but progressively more brittle behavior. At 20 wt% and

30 wt%, the the tensile strength reduced to 28.3 MPa (MX_{20}) and 25.5 MPa (MX_{30}). Correspondingly, the strain at break decreased to 3.8% and 2.1%. Toughness dropped to 0.71 and 0.30 $MJ \cdot m^{-3}$, reflecting the diminishing capacity for plastic deformation. At the highest loading of 50 wt% MXene, the strength fell to only 18.2 MPa, and the elongation at break decreased to 0.8%, yielding a toughness of just 0.073 $MJ \cdot m^{-3}$. This brittle failure mode reflects the dominance of MXene flakes within the composite, where strong filler–filler interactions hinder matrix chain mobility and accelerate crack propagation under load [13, 14]. The results indicate a clear trade-off between stiffness and toughness with increasing MXene content. While the polymer-rich films retain flexibility and high energy absorption, the MXene-rich films achieve superior modulus but at the expense of ductility. Such a tunable mechanical response suggests that MXene/PVDF-HFP films can be tailored for specific applications: high-load fractions for structural integrity and stiffness, or lower fractions for flexible, foldable, and energy-absorbing devices.

Despite these losses in elongation, the composites retained remarkable macroscopic flexibility. As illustrated in Figure 3b, the MX_{30}/P film can withstand severe mechanical deformations, including twisting, folding, and origami-inspired shaping into a crane, without visible cracking or delamination. This apparent discrepancy between reduced tensile strain and preserved foldability suggests that the films accommodate local deformations through strong interfacial bonding between MXene sheets and the polymer host. This result reveals that MXene/PVDF-HFP composites exhibit a dual mechanical character: they combine tunable tensile stiffness and strength with exceptional macroscopic foldability. The unique balance demonstrated here is particularly promising for applications in flexible and foldable electronics, wearable devices, and origami-inspired energy storage systems, where both mechanical robustness and conformability are critical.

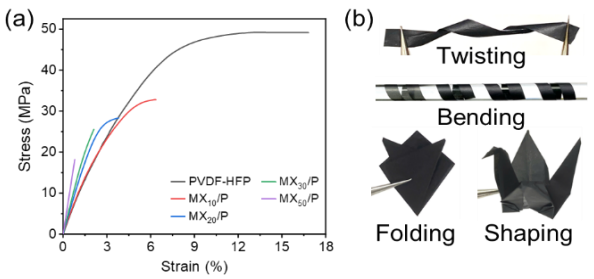

Figure 3. *(a) Stress-strain curves of the PVDF-HFP and MXn/P films, (b) Digital photos of MX30/P film with different mechanical deformations*

3.3. Electrical conductivity and EMI shielding performance

The electrical conductivity of MXene/PVDF-HFP composites exhibited a sharp percolation-type transition as the MXene content increased (Figure 4a). At a loading of 10 wt%, the films displayed only modest conductivity (1.71 ± 0.41 $S \cdot m^{-1}$), suggesting that MXene sheets were still isolated within the insulating polymer host. Increasing the loading to 20 wt% enhanced the conductivity by an order of magnitude to 19.7 ± 0.45 $S \cdot m^{-1}$, indicating the onset of conductive network formation. A dramatic jump occurred at 30 wt%, where the conductivity reached 395.8 ± 7.9 $S \cdot m^{-1}$, nearly two orders of magnitude higher than at 20 wt%. This behavior is characteristic of a percolation threshold near ~25–30 wt%, where previously disconnected flakes overlap to form continuous electron pathways. At 50 wt%, the conductivity reached 2174.7 ± 166 $S \cdot m^{-1}$, consistent with a dense, highly interconnected MXene network dominating charge transport. The strong dependence of σ on filler loading underscores the central role of interflake tunneling and sheet overlap in establishing electrical conduction.

The functional impact of the percolation-driven conductivity enhancement is further illustrated by the LED illumination experiment (Figure 4b). In the absence of any film, the electrical circuit remains open and the LED stays unlit, confirming the insulating nature of the setup. Incorporation of MX_{10}/P films enables a weak but visible LED illumination, consistent with the low conductivity at this filler loading. A substantial increase in brightness is observed for the MX_{30}/P film, directly reflecting the nearly three orders-of-magnitude rise in conductivity to ~396 $S \cdot m^{-1}$. The LED reaches full, stable illumination when integrated with MX_{50}/P films, where the conductivity exceeds ~2×10^3 $S \cdot m^{-1}$. This simple yet powerful demonstration confirms that percolated MXene networks not only raise bulk conductivity but also deliver macroscopic current-handling capability sufficient for powering low-voltage devices, highlighting the practical potential of MXene/polymer films in flexible electronics.

The EMI shielding efficiency (SE) of the MX_n/P films (8–12.5 GHz) followed the same trend as conductivity (Figure 4c). Neat PVDF-HFP showed negligible attenuation across the band, confirming its insulating character. Incorporation of 10 wt% MXene increased SE to a nearly frequency-independent value of 8 dB (at 10 GHz), arising from the initial reflection of incident waves by conductive flakes and ohmic losses within local clusters. At 30 wt%, SE rose to approximately 25 dB, crossing the threshold for practical EMI shielding materials (>20 dB). This increase stems from both stronger reflection and enhanced absorption as multiple internal reflections occur between parallel MXene lamellae. At 50 wt%, the films reached an SE of about 36 dB across the X-band, equivalent to over 99.97% attenuation of incident radiation, placing these films in the class of high-performance thin-film EMI shields.

The correlation between σ and SE demonstrates that conductivity governs reflection-dominated shielding, while the layered MXene morphology amplifies absorption through multiscattering pathways. At low filler contents, where conductivity is insufficient to sustain extended pathways, SE is modest. Beyond the percolation threshold, the emergence of continuous MXene stacks not only improves charge transport but also creates layered conductive/dielectric interfaces that facilitate both reflection and absorption. The polymer host contributes dielectric loss and mechanical integrity while preventing MXene agglomeration, thereby stabilizing the shielding performance [15].

The EMI shielding mechanism is schematically illustrated in Figure 4d. When incident electromagnetic waves strike the MX_n/P composites, the high electronic conductivity of the interconnected MXene networks induces strong surface currents that reflect a significant portion of the radiation. Simultaneously, the layered MXene nanosheets and interfacial boundaries within the polymer matrix promote multiple internal reflections, effectively prolonging the propagation path. This extended path length allows enhanced dissipation of electromagnetic energy via ohmic losses and interfacial polarization, leading to efficient absorption. At higher MXene contents (≥30 wt%), absorption becomes the dominant shielding contribution, as evidenced by the continuous conductivity networks and the frequency-stable EMI SE response. The coexistence of reflection and absorption ensures broadband attenuation, while the lightweight and flexible polymeric framework enables mechanical compliance, making these composites highly attractive for next-generation portable and wearable shielding technologies.

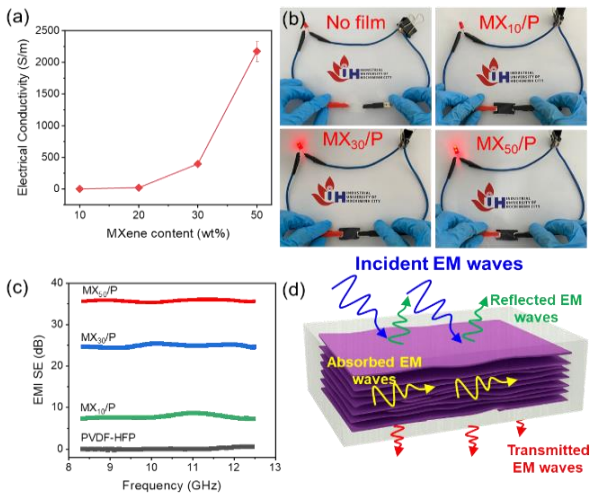

Figure 4. *(a) Electrical conductivity of MXn/P film, (b) LED illumination using PVDF-HFP film and MX_n/P films, (c) EMI SE of PVDF-HFP film and MX_n/P films, (d) EMI shielding mechanism*

To place the obtained EMI shielding performance in context, the results were compared with previously reported composites based on representative 2D nanomaterials such as graphene and carbon nanotubes (CNTs). Graphene-based polymer composites typically exhibit total EMI shielding effectiveness (SE_t) values in the range of 20–35 dB [16–18], while CNT/polymer composites generally achieve <30 dB [19, 20]. In this study, our composite demonstrates an SE_t of 36 dB at a filler loading of 50 wt%, which surpasses or matches many reported 2D material systems while maintaining excellent flexibility, low density, and enhanced fire resistance.

To further validate the EMI shielding performance under real-world conditions, demonstrations were carried out using a commercial smart watch (Figure 5a) and an EMF (electromagnetic field) meter (Figure 5b).

When a pristine PVDF-HFP film was interposed between the smart watch and the hand, the smart watch could measure the heart rate. In stark contrast, the MX_{50}/P films, and the Al film were placed between the smart watch and hand, effectively suppressing wireless transmission, resulting in unable measurement of heart rate. The EMF meter can measure the intensity of the electromagnetic field which is generated from electronic devices such as laptops and computers. In the absence of shielding, the EMF meter placed near a laptop shows an intensity of 179 V/m (Figure 5b). Upon introducing MX_{50}/P films, and Al film, the EMF signal dropped precipitously, eventually approaching the noise floor of the instrument, thereby confirming attenuation exceeding 99.9%.

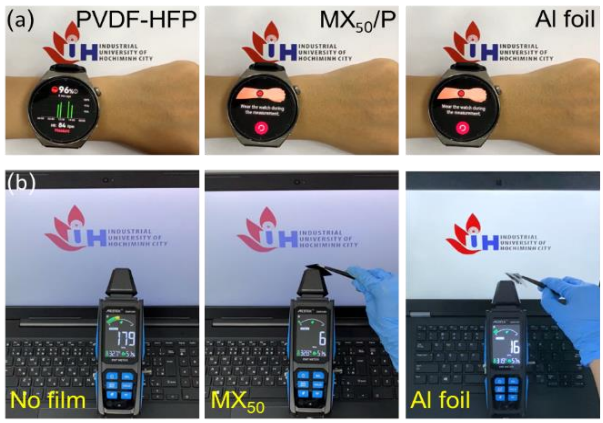

Figure 5. *EMI shielding demonstration of PVDF-HFP film and MXn/P films using (a) Smart watch, (b) EMF Meter*

These experimental demonstrations bridge the gap between laboratory metrics and real-world applicability, confirming that MXene/PVDF-HFP films are not only lightweight and flexible but also capable of delivering robust EMI protection in practical device environments. This combination of electrical conductivity, EMI SE, and real-world effectiveness positions the composites as strong candidates for next-generation flexible shielding in wearable, IoT, and aerospace systems.

3.4. Flame retardancy

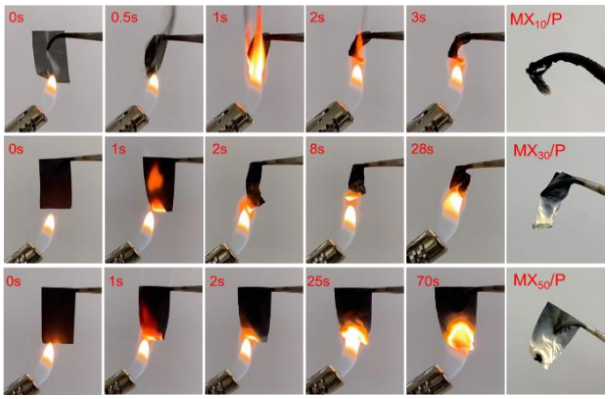

Figure 6. *Flame retardancy of MX_n/P films*

Figure 6 shows that sequential optical images illustrate the burning behavior of MX_{10}/P, MX_{30}/P, and MX_{50}/P films at designated time intervals, together with the final residues after combustion. For MX_{10}/P, ignition occurs almost instantaneously (~0.5 s), and rapid flame spread leads to severe structural collapse within 3 s, leaving a brittle, charred residue. In MX_{30}/P, ignition is delayed to ~2 s and the flame propagates more slowly; localized shrinkage and partial carbonization are observed, with the

sample retaining partial structure after 28 s of exposure. By contrast, MX_{50}/P demonstrates remarkable flame retardancy: despite continuous flame impingement for up to 70 s, the film resists complete combustion, showing progressive surface charring and self-extinguishing tendencies while preserving most of its shape. These results highlight that increasing MXene loading enhances thermal stability, promotes char formation, and effectively suppresses catastrophic flame spread, thereby endowing the MX_n/P composites with superior fire resistance compared to the pristine polymer matrix.

4. Conclusion

In summary, we have demonstrated a fluoride-free molten salt strategy to synthesize $Ti_3C_2T_x$ MXene nanosheets and incorporated them into PVDF-HFP matrices to engineer multifunctional EMI shielding composites. The chloride-terminated MXenes not only preserved crystallinity and layered morphology but also dispersed uniformly within the polymer host, forming conductive networks that drove a dramatic percolation transition in electrical conductivity. As a result, the MX_n/P composites achieved EMI SE values up to 36 dB in the X-band, equivalent to >99.97% attenuation, while retaining flexibility and foldability essential for wearable devices. Practical demonstrations confirmed their ability to suppress wireless signals in smart watches and reduce EMF emissions from laptops to near-background levels. Beyond EMI shielding, the composites also exhibited enhanced flame retardancy, with MX_{50}/P films resisting sustained combustion and displaying self-extinguishing behavior. These results underscore the synergy between MXene nanosheets and PVDF-HFP, yielding a platform material that is lightweight, mechanically compliant, electrically conductive, and fire-resistant. By bridging scalability, multifunctionality, and practical performance, the MX_n/P composites reported here offer a compelling pathway toward next-generation EMI shielding solutions for wearable electronics, IoT systems, and aerospace technologies.

Acknowledgement: The authors appreciate financial support from the National Foundation for Science and Technology Development (NCUD.02-2022.34).

REFERENCES

[1] B. Shen, W. Zhai, and W. Zheng, "Ultrathin Flexible Graphene Film: An Excellent Thermal Conducting Material with Efficient EMI Shielding", *Advanced Functional Materials*, vol. 24, no. 8, pp. 4542-4548, 2024. https://doi.org/10.1002/adfm.201400079

[2] D. Mani *et al.*, "Stretching Induced Alignment of Graphene Nanoplatelets in Polyurethane Films for Superior In-Plane Thermal Conductivity and Electromagnetic Interference Shielding", *Carbon*, vol. 201, pp. 568-576, 2023. https://doi.org/10.1016/j.carbon.2022.09.047.

[3] D. K. Nguyen *et al.*, "Thermoconductive Graphene Fluoride Cross-Linked Aramid Nanofiber Composite Films with Enhanced Mechanical Flexibility and Flammable Retardancy for Thermal Management in Wearable Electronics", *ACS Applied Nano Materials,* vol. 7, no. 3, pp. 2724-2734, 2023. https://pubs.acs.org/doi/10.1021/acsanm.3c04771

[4] S. Anand *et al.*, "A continuous interfacial bridging approach to fabricate ultrastrong hydroxylated carbon nanotubes intercalated MXene films with superior electromagnetic interference shielding and thermal dissipating properties", *Advanced Composites and Hybrid Materials,* vol. 7, no. 33, 2024. https://doi.org/10.1007/s42114-024-00842-5

[5] J. B. Kim *et al.*, "Multilayered graphene fluoride and Ti3C2Tx MXene-based aramid nanofiber films with excellent thermal conductivity and electromagnetic interference shielding performance", *Colloids and Surfaces A: Physicochemical and Engineering Aspects,* vol. 685, no. 133121, pp. 1-12, 2024. https://doi.org/10.1016/j.colsurfa.2023.133121

[6] A. Iqbal, T. Hassan, Z. Gao, F. Shahzad, and C. M. Koo, "MXene-incorporated 1D/2D nano-carbons for electromagnetic shielding: A review", *Carbon*, vol. 203, pp. 542-560, 2023. https://doi.org/10.1016/j.carbon.2022.11.104.

[7] D. D. Kruger, H. García, and A. Primo, "Molten Salt Derived MXenes: Synthesis and Applications", *Advanced Science*, vol. 11, no. 2307106, pp. 1-29, 2024. https://doi.org/10.1002/advs.202307106

[8] Y. Zhang *et al.*, "Core-shell engineering of graphite nanosheets reinforced PVDF toward synchronously enhanced dielectric properties and thermal conductivity", *European Polymer Journal*, vol. 215, no. 113236, 2024. https://doi.org/10.1016/j.eurpolymj.2024.113236.

[9] L. Liu *et al.*, "Exfoliation and Delamination of Ti3C2Tx MXene Prepared via Molten Salt Etching Route", *ACS Nano*, vol. 16, pp. 111-118, 2022. DOI: 10.1021/acsnano.1c08498

[10] T. Zhou *et al.*, "Super-tough MXene-functionalized graphene sheets", *Nature Communications*, vol. 11, no. 1, article no. 2077, 2020. https://doi.org/10.1038/s41467-020-15991-6

[11] S. Xu, G. Wei, J. Li, W. Han, and Y. Gogotsi, "Flexible MXene–graphene electrodes with high volumetric capacitance for integrated co-cathode energy conversion/storage devices", *Journal of Materials Chemistry A,* vol. 5, pp. 17442-17451, 2017. https://doi.org/10.1039/C7TA05721K

[12] J. Q. Luo, S. Zhao, H. B. Zhang, Z. Deng, L. Li, and Z. Z. Yu, "Flexible, stretchable and electrically conductive MXene/natural rubber nanocomposite films for efficient electromagnetic interference shielding", *Composites Science and Technology*, vol. 182, no. 31, article no. 107754, 2019. https://doi.org/10.1016/j.compscitech.2019.107754

[13] A. Ahmed *et al.*, "Two-dimensional MXenes: New frontier of wearable and flexible electronics", *InfoMat*, vol. 4, no. 4, article no. e12295, 2022. https://doi.org/10.1002/inf2.12295

[14] Q. Gao, Y. Pan, G. Zheng, C. Liu, C. Shen, and X. Liu, "Flexible multilayered MXene/thermoplastic polyurethane films with excellent electromagnetic interference shielding, thermal conductivity, and management performances", *Advanced Composites and Hybrid Materials*, vol. 4, pp. 274-285, 2021. https://doi.org/10.1007/s42114-021-00221-4

[15] P. Song, B. Liu, H. Qiu, X. Shi, D. Cao, and J. Gu, "MXenes for polymer matrix electromagnetic interference shielding composites: A review", *Composites Communications*, vol. 24, no. 100653, 2021. https://doi.org/10.1016/j.coco.2021.100653

[16] K. Sabira, M. P. Jayakrishnan, P. Saheeda, and S. Jayalekshmi, "On the absorption dominated EMI shielding effects in free standing and flexible films of poly(vinylidene fluoride)/graphene nanocomposite", *European Polymer Journal*, vol. 99, pp. 437-444, 2018. https://doi.org/10.1016/j.eurpolymj.2017.12.034

[17] V. Eswaraiah, V. Sankaranarayanan, and S. Ramaprabhu, "Functionalized Graphene–PVDF Foam Composites for EMI Shielding", *Macromolecular Materials and Engineering,* vol. 296, pp. 894-898, 2011. https://doi.org/10.1002/mame.201100035

[18] G. S. Wang, X. J. Zhang, Y. Z. Wei, S. He, L. Guo, and M. S. Cao, "Polymer composites with enhanced wave absorption properties based on modified graphite and polyvinylidene fluoride", *Journal of Materials Chemistry A*, vol. 1, pp. 7031-7036, 2013. https://doi.org/10.1039/C3TA11170A

[19] R. Kumaran, S. D. Kumar, N. Balasubramanian, M. Alagar, V. Subramanian, and K. Dinakaran, "Enhanced Electromagnetic Interference Shielding in a Au–MWCNT Composite Nanostructure Dispersed PVDF Thin Films", *Journal of Physical Chemistry C*, vol. 120, no. 25, pp. 13771-13778, 2016. https://doi.org/10.1021/acs.jpcc.6b01333

[20] M. Sharma, M. P. Singh, C. Srivastava, G. Madras, and S. Bose, "Poly(vinylidene fluoride)-Based Flexible and Lightweight Materials for Attenuating Microwave Radiations", *ACS Applied Materials & Interfaces*, vol. 6, no.23, pp. 21151-21160, 2014. https://doi.org/10.1021/am506042a